# EXAUST PLUME EFFECT OF WINGED TWO-STAGE-TO-ORBIT SEPARATION AT ASCENT USING AERODYNAMIC-FLIGHT DYNAMICS TECHNIQUE

**Hiroya Iwafuji***
***Department of Aerospace Engineering, Faculty of System Design, Tokyo Metropolitan University**

**Keywords**: *Two-stage-to-orbit, Plume effect, Hypersonic, CFD, Separation phase*

## Abstract

*This paper discusses flowfield around the winged two-stage-to-orbit (TSTO) at staging phase in view of the engine plume effect using a computational fluid dynamics and flight dynamics. In this TSTO model, a suborbital rocket was adopted owing to its similarity in shape to an orbiter and booster, consisting of a main wing, V-tail, nine nozzles on the booster, and two nozzles on the orbiter. An unstructured mesh based flow solver was applied to the staging simulation of the TSTO with consideration of the engines plume. According to numerical results, the effects of freestream-plume interaction and the shock-shock phenomena at the separation were investigated by varying the free-stream velocity, angle of attack, and relative position between the orbiter and booster. In addition, the engine plume effects and separation trajectory were discussed by comparing with the powered and unpowered TSTO aerodynamic data and its flowfield. The separation trajectory was calculated using an aerodynamic-flight dynamics simulation. As a result, separation feasibility is investigated and simulated in the trajectory that there has no re-contact between booster and orbiter.*

## 1 Introduction

The winged reusable sounding rocket (WIRES) [1] as shown in Fig. 1 has been developed by the research and development teams of the Kyusyu Institute of Technology. In our future plan it will be extend to a two-stage-to-orbit (TSTO) consisting of an orbiter and a booster as a future concept [2]. Figure 2 illustrates the current TSTO concept and the assumed flight sequence. In this concept, the flowfield around the TSTO should be complicated at the ascent because this TSTO consists of both the reusable orbiter/booster, which has a wing, body, and V-tail. It should especially be investigated during the separation in the whole phase of the TSTO. To design the control technique of TSTO at the separation, the orbiter/booster's motion without any control should be well understood. In terms of aerodynamic analysis, computational fluid dynamics (CFD) is required because an experiment using two vehicles at hypersonic will take high cost to conduct. Thus, its flowfield and motion are simulated using aerodynamics and flight dynamics in considering with the effect of the exhaust plume of both the orbiter/booster to investigate the separation feasibility.

**Fig. 1. WIRES [1].**

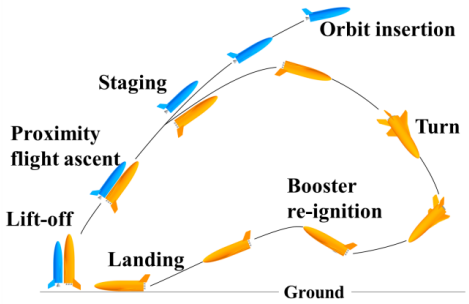


**Fig. 2. Flight sequence of TSTO.**

## 2 Review of TSTO Concept Including Bell Nozzle Designs

The TSTO specifications are shown in Fig. 3 [2]. For the exhaust plume calculation, the nozzles are attached on the aft bodies. In this study, bell nozzles are designed as shown in Fig. 4 with the parabolic method by G. V R. Rao [3] to install the TSTO concept in [2]. Its flow conditions are calculated at the nozzle exit using the static pressure $P_e$, static temperature $T_e$, and exhaust velocity $V_e$, as shown in Table 1 [2].

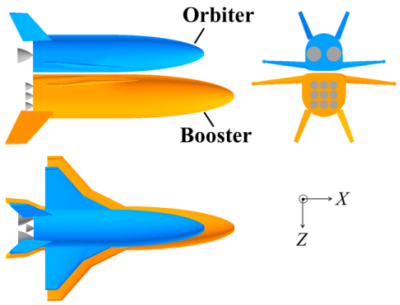


**Fig. 3. Winged TSTO specifications.**

**Table 1. TSTO specifications.**

| | |
|---|---|
| Total gross mass [t] | 870.0 |
| Payload mass [t] | 10.0 |
| Booster body length [m] | 40.8 |
| gross mass [t] | 661.6 |
| Orbiter body length [m] | 34.7 |
| gross mass [t] | 209.1 |

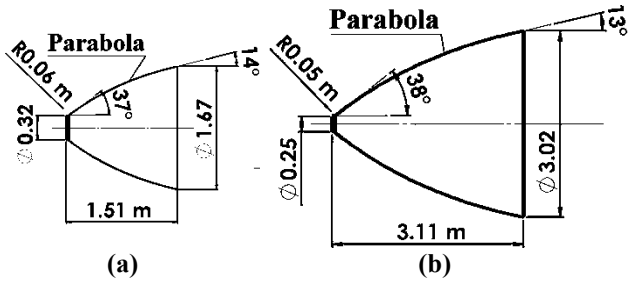


**Fig. 4. Designed nozzles.**
**(a) Booster, (b) Orbiter.**

**Table 1. Nozzle specifications [2].**

| Quantity | | Booster | Orbiter |
|---|---|---|---|
| Number of units | | 9 | 2 |
| Expansion ratio | | 26.9 | 146.5 |
| Oxidizer-to-fuel mass ratio | | 3.49 | 3.73 |
| Plume conditions at nozzle exit | Pressure [kPa] | 32.75 | 3.55 |
| | Mach number | 3.63 | 4.55 |
| | Temperature [K] | 1393.4 | 899.46 |
| | Density [kg/m$^3$] | 0.063 | 0.011 |
| | Specific heat ratio | 1.4 | 1.4 |

## 3 Computational Conditions for Flowfield Around Ascent and Stage Separation

Table 2 shows simulated flight conditions at ascent of TSTO which Mach number $M$ = 0.4 to 6.8. At Case 1 in Table 2, booster engine is powered. At Case 2 and 3, both engines are powered. Case 4 is simulated as the staging separation. The conditions of Reynolds number, $Re = 2.83\times10^6$, $M$ = 6.8 is assumed at the separation of 40 km. The gas constant, $R$ = 287.1 [J / (kg·K)], specific heat ratio $\gamma$ = 1.4, and atmospheric model is constructed based on the U.S. standard atmosphere 1976 [4]. The stage separation variables with the relative separation distances, $\Delta x, \Delta z$, and relative Euler angular orientaions,$\theta$ are defined in Fig. 5.

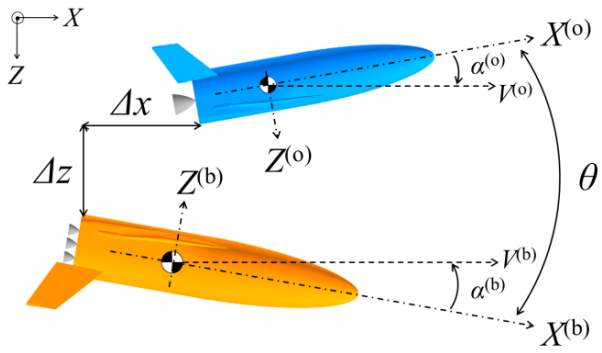


**Fig. 5. Definition of stage separation variables.**

**Table 2. Simulated flight conditions.**

| Case | Mach number | Altitude [km] | Booster engine mode | Orbiter engine mode |
|---|---|---|---|---|
| 1 | 0.4 | 2.0 | Powered | Unpowered |
| 2 | 4.0 | 28.3 | Powered | Powered |
| 3 | 6.8 | 40.5 | Powered | Powered |
| 4 | 6.8 | 40.5 | Unpowered | Powered |

## 4 Computational Methods

### 4.1 Computational Fluid Dynamics

An unstructured mesh-based CFD is employed. In this study, the Reynolds-averaged Navier–Stokes simulation is conducted by employing the shear–stress transport–2003sust [5] as a turbulence model, the Harten–Lax–Van Leer–Eingeld [6] for an inviscid flux calculation, and the lower-upper symmetric Gauss–Seidel [7] for the time integration. For the CFD calculation,

approximately 7 million nodes of unstructured mesh as shown in Fig. 6 are used. The minimum grid spacing is 55.7 [μm] at $y^+ = 1.0$. We used the FAST aerodynamic routines [8] developed by the Japan Aerospace Exploration Agency as a CFD solver and the mixed-element grid generator in three dimensions (MEGG3D) [9] [10] , as an unstructured mesh solver.

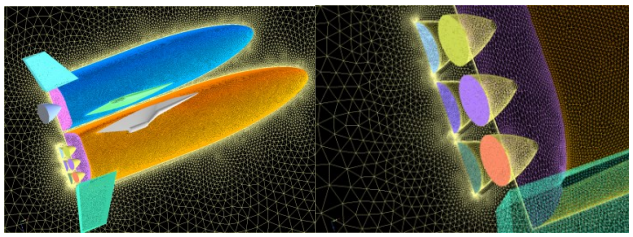

(a) (b)

**Fig. 6. Calculation mesh**
**(a) Overview, (b) Booster nozzle close-up.**

## 4.2 Flight Dynamics Solutions

For the trajectory simulation at the stage separation, a flight dynamics technique is solved with a three-degrees-of-freedom equation of motion by 4th order Runge-Kutta method [11]. The fluid-orbit coupling calculation for the TSTO separation is simulated as shown in Fig. 7.

(a) Calculate the aerodynamic coefficient at the initial location by CFD solutions.

(b) Simulate the locations at $t_{i+1} = t_i + \Delta t$ by flight dynamics solutions.

(c) Regenerate the mesh by updated booster/orbiter locations. This paper discusses in 2 seconds of separation.

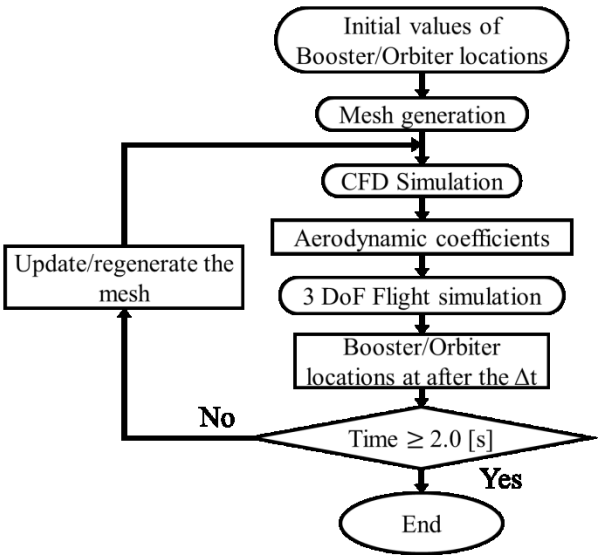


**Fig. 7. Flowchart of the aerodynamics-fluid dynamics simulation.**

## 5 Results and Discussions

### 5.1 Flowfield Around Isolated Vehicle (Booster)

Figure 8 illustrates the comparison of the powered and unpowered $C_D$ – Mach number. The plume affects the back surface pressure and hence the $C_D$ value. In subsonic flow, the powered flow with plume shows a higher $C_D$ than the unpowered one. On the contrary, in supersonic flow, the powered flow with plume shows a lower $C_D$ than the unpowered one. These phenomena are due to the difference of $C_p$ on aft fuselages. Figures 9 (a), (b) and 10 (a), (b) compares the powered and unpowered booster's aft fuselages by showing the pressure coefficients contour at $M = 0.4, 4.0$. The results of these Figs indicate the same relations between powered and unpowered of Fig. 8.

Another potential adverse impact of engine plumes shown in Fig. 11 (a) is the effects of plume-induced flow separation (PIFS) on nozzles and on the fuselage only where plume shocks impinge. The PIFS effect can only be determined with viscous simulations. This effect will increase the portion of airframe (aft fuselage, primary wings, V-tails and nozzles) that is engulfed by engine plumes. Additionally, shock waves interacting with boundary layers may cause flow separation.

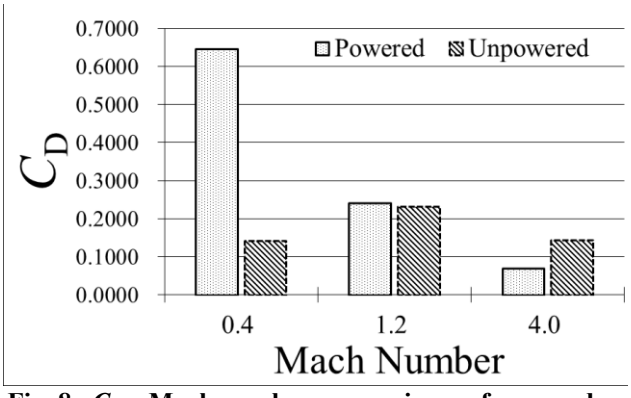


**Fig. 8. $C_D$ – Mach number comparisons of powered and unpowered booster.**

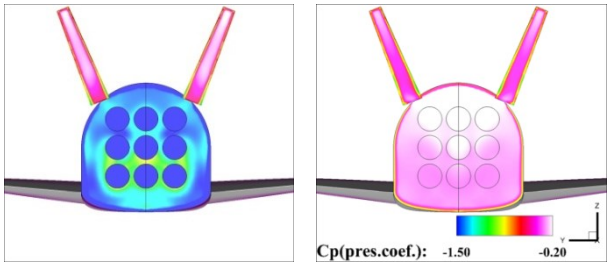


(a) (b)

**Fig. 9. $C_p$ contours on booster aft fuselage at $M$ = 0.4.**
**(a) Powered, (b) Unpowered.**

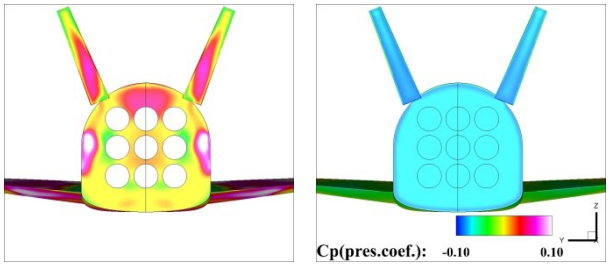


(a) (b)

**Fig. 10. $C_p$ contours on booster aft fuselage at $M$ = 4.0.**
**(a) Powered, (b) Unpowered.**

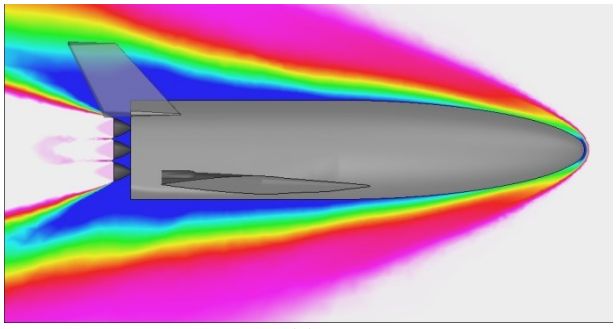

(a)

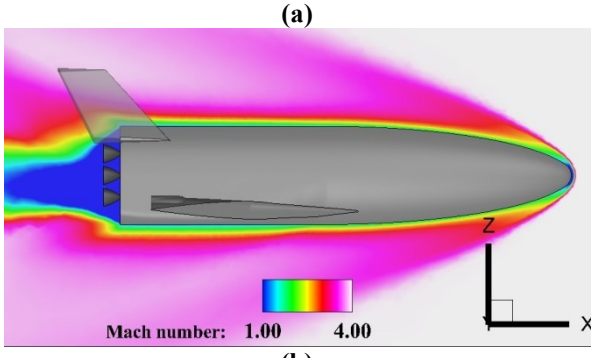


(b)

**Fig. 11. Booster flow field shown by Mach number contour at $M$ = 4.0.**
**(a) Powered, (b) Unpowered.**

## 5.2 Flowfield Around TSTO at Ascent

Figure 12 shows the TSTO flow field at $M$ = 0.4 (Case 1), 4.0 (Case 2) and 6.8 (Case 3) by the Mach number contour on the $y$ = -0.2 cutting plane. The aerodynamic interaction between the booster/orbiter primary wings and ambient-plume flow can be observed. A PIFS effect can be confirmed in supersonic flow. At aft body, shock waves interacting with boundary layers may cause flow separation.

Figure 13 compares $C_D$ with booster/orbiter powered and unpowered simulations. The effects in this flow field beyond supersonic, plume interaction decreases $C_D$.

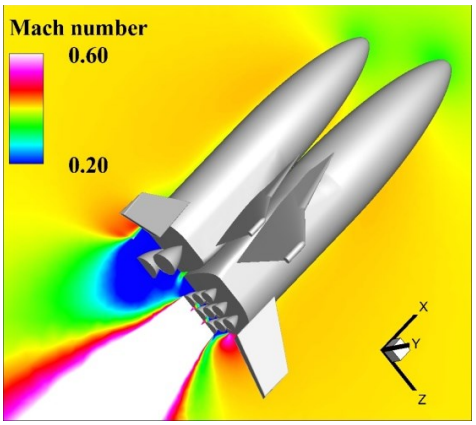


(a)

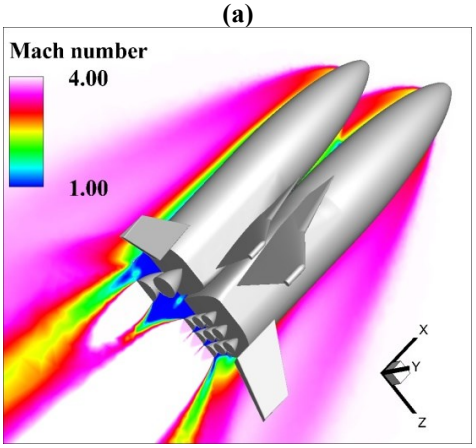


(b)

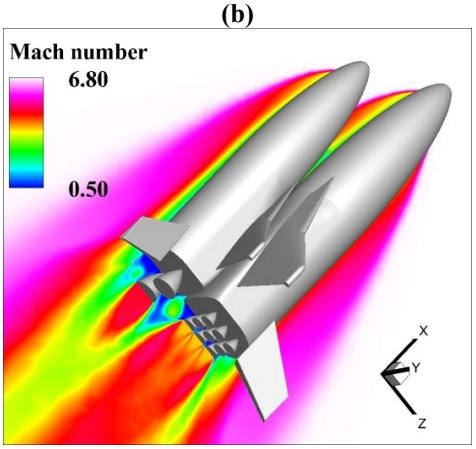


(c)

**Fig. 12. TSTO flow field at ascent flight.**
**(Mach number contour on $y$ = -0.2 cutting plane)**
**(a) $M$ = 0.4 in Case 1, (b) $M$ = 4.0 in Case 2,**
**(c) $M$ = 6.8 in Case 3.**

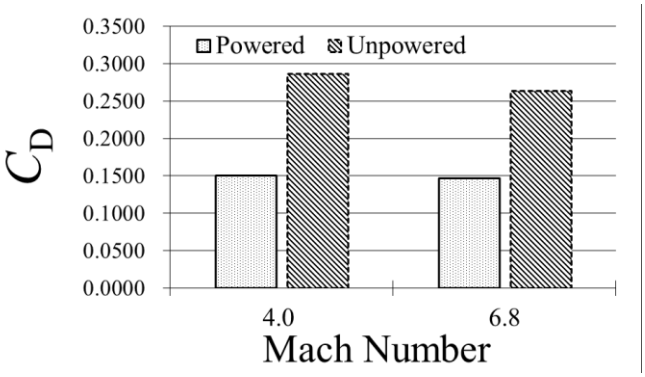


**Fig. 13. $C_D$ – Mach number comparisons of powered and unpowered TSTO at $M$ = 4.0, 6.8.**

## 5.3 Staging Separation

Staging separation was simulated as the condition of Case 4 in Table 2. We simulated 2 different initial $\Delta z$=0.445, 2.225 [m] positions.

In Fig. 14, initial $\Delta z$=0.445[m], there were re-contacted at front between orbiter/booster at 0.20 [s]. This collision was mainly caused by orbiter and booster's $C_M$ decreases. In terms of flow field as shown in Fig. 15, the distance between orbiter and booster was too short and the airflow between orbiter and booster was interacted to both lower surfaces by several times of shock wave reflections. $C_M$ decreasing is in particular affected by the interaction between orbiter/booster's primary wings. The interaction leads to pressure increases of both lower wings and it results in $C_M$ decreases. In order to separate successfully without any collision or unexpected motion, giving larger $C_M$ to both orbiter/booster is needed by separation equipment such as joint mechanisms. Thus, to investigate separation feasibility, external moment was applied to orbiter/booster's center of gravity (CG). In Fig. 16, initial $\Delta z$ =2.225[m], this simulation was forcibly add the $C_{Madd}$ = + 0.80 at the orbiter's CG. As a result, there were successful separation in 2.00 [s]. Figure 17 shows the flow field at 1.50 [s] on separating. High pressured zone at primary wing is confirmed.

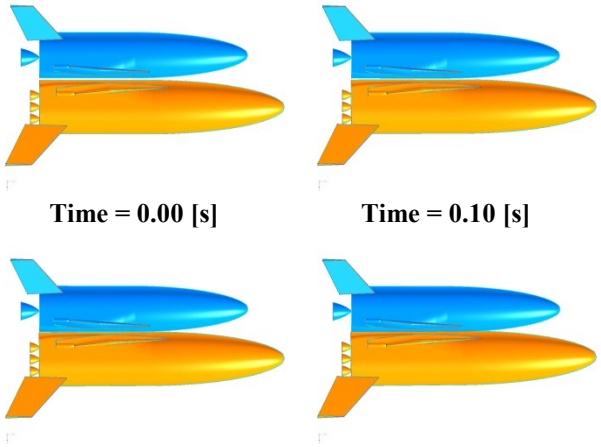


**Fig. 14. Separation trajectory (initial $\Delta z$ = 0.445 [m]).**

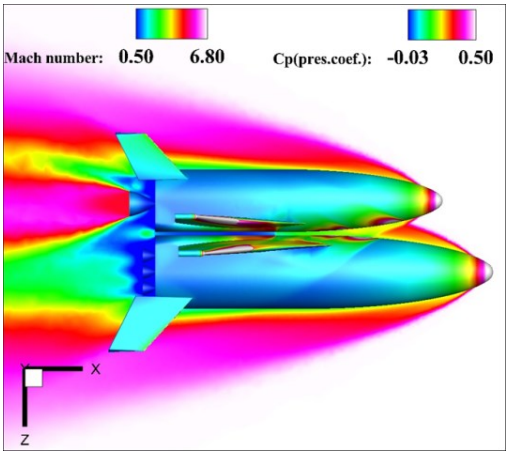


**Fig. 15. TSTO flow field in Case 4 (Time = 0.00 [s], initial $\Delta z$ = 0.445 [m]).**
**(Contours of pressure coefficient on the surface and Mach number on $y$ = -0.2 cutting plane)**

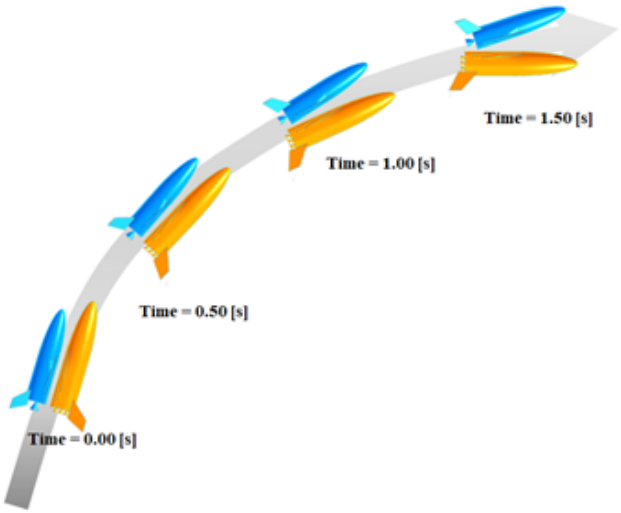


**Fig. 16. Separation trajectory applied $C_{Madd}$ = 0.80 at orbiter's CG (initial $\Delta z$ = 2.225 [m]).**

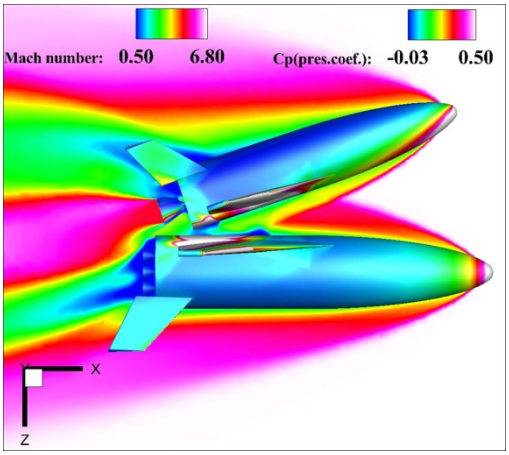


**Fig. 17. TSTO flow field in Case 4 (Time = 1.50 [s], initial $\Delta z$ = 2.225 [m]). (Contours of pressure coefficient on the surface and Mach number on $y$ = -0.2 cutting plane)**

## 6 Conclusions

The effect of the exhaust plume on the aerodynamics and flight dynamics of both the orbiter/booster at the ascent-separation was considered with discussing the separation feasibility. To separate without any control could not be succeeded. Separation equipment to give the $C_M$ and to keep the distance between orbiter/booster must require for the separation. Each stage of the proximity flight, engine plume affects to TSTO aerodynamic coefficient and its trajectory. For future research, we need to develop the databases of changing relative locations between orbiter/booster and angle of attack. In addition, separation equipment such as designing and optimizing joint mechanisms should be considered.

## 7 Acknowledgements

I would like to thank K. Yonemoto and T. Fujikawa in Kyushu Institute of Technology for providing the winged reusable sounding rocket (WIRES) data and suggesting the topic treated in this paper. I am grateful to M. Kanazaki for carefully proofreading the manuscript.

This work is supported by "Joint Usage/Research Center for Interdisciplinary Large-scale Information Infrastructures" in Japan (Project ID: jh180057-NAJ).

## References

[1] Yonemoto, K. et al., *Winged Test Rocket with Fully Autonomous Guidance and Control for Realizing Reusable Suborbital Vehicle*, International Journal of Mechanical, Aerospace, Industrial, Mechatronic and Manufacturing Engineering, 10, 1, 96–107 (2016)

[2] T. Fujikawa, K. Yonemoto, et al., *Research and Development of Winged Reusable Rocket: Current Status of Experiment Vehicles and Future Plans*, Asia-Pacific International Symposium on Aerospace Technology, I5-3 (2017)

[3] G. V R. Rao, *Exhaust Nozzle Contour for Optimum Thrust*, Journal of Jet Propulsion, 28, 6, 377-382 (1958)

[4] *U. S. standard atmosphere*, National Ocean and Atmospheric Administration, National Aeronautics and Space Administration, United States Air Force (1976)

[5] Florian Menter, *Improved Two-Equation k-omega Turbulence Models for Aerodynamic Flows*, NASA TM 103975 (1992)

[6] B. Einfeldt, *On Godunov-Type Methods for Gas Dynamics*, SIAM Journal on Numerical Analysis, 25, 294-318 (1988)

[7] Seokkwan Yoon, Antony Jameson, *Lower-Upper Symmetric-Gauss-Seidel Method for the Euler and Navier-Stokes Equations*, AIAA, 26, 9 (1988)

[8] A. Hashimoto, K. Murakami, et al., *Paulus Lahur Toward the Fastest Unstructured CFD Code 'FaSTAR'*, AIAA, 1075 (2012)

[9] Y. Ito, M. Murayama, K. Yamamoto, *Efficient Hybrid Surface/Volume Mesh Generation Using Suppressed Marching Direction Method*, AIAA J., 51, 6, 1450-1461 (2013)

[10] Y. Ito, et al., *Direct Surface Triangulation Using Stereolithography Data*, AIAA J., 40, 3, 490-496 (2002)

[11] J. C. Butcher, *A history of Runge-Kutta methods*, Applied Numerical Mathematics 20, 247-260 (1996)

## 8 Contact Author Email Address

To get in contact with the authors, please refer to the following email addresses:
iwafuji-hiroya@ed.tmu.ac.jp

## Copyright Statement